Research Square

Preprints are preliminary reports that have not undergone peer review.
They should not be considered conclusive, used to inform clinical practice,
or referenced by the media as validated information.

Relational reduction protects massless spin-2 modes in a programmable quantum network

Shalender Singh

singhshalender@gmail.com

Independent Researcher https://orcid.org/0000-0003-3677-4043

Vishnu Priya Singh Parmar

Independent Researcher

Article

Keywords:

Posted Date: August 22nd, 2026

DOI: https://doi.org/10.21203/rs.3.rs-10677044/v1

License: This work is licensed under a Creative Commons Attribution 4.0 International License.
Read Full License

Additional Declarations: There is **NO** Competing Interest.

Relational reduction protects massless spin-2 modes in a programmable quantum network

immediate

August 12, 2026

Abstract

Positive quantum response metrics seem incompatible with the indefinite scalar direction of covariant spin-2 actions. We establish a transferable design rule that removes this obstacle before a continuum limit is taken. A positive full-rank quantum chart is equipped with an exact relational complex; its response is reduced to a two-dimensional cohomology; and the complete finite spectral kernel is tested before any derivative expansion. We prove that positive and covariant representatives then differ only by a quadratic form in the imposed constraint, and that Gaussian quantum feedback preserves the quotient, masslessness and physical spectral measure. The theorem holds for arbitrary finite exact complexes of the stated form and passes 3,000 randomized tests with chart condition numbers up to 10^{10}. An eight-route, four-port unitary network supplies an explicit realization with a positive six-coordinate Gram chart, two tensor modes and a Stieltjes-positive response. We give a five-qubit closed-time-path protocol requiring 57 native entanglers on an all-to-all architecture, with quantitative gates for helicity degeneracy, subthreshold noise, residue positivity and root–threshold interlacing. The protocol tests relational protection directly, without requiring a gravitational interpretation.

Positive susceptibilities are a basic feature of quantum statistical and information geometry. Covariant descriptions of a massless spin-2 field, however, contain an off-shell scalar direction with the opposite sign[1, 2]. This mismatch is often treated as evidence that a positive quantum metric cannot generate healthy gravitational dynamics without an independently imposed Lorentzian action. The difficulty also appears in quantum simulation: a finite unitary processor naturally produces positive probabilities and covariances, whereas the desired constrained field theory is usually written in an indefinite redundant space.

The sign conflict is avoidable. The scalar direction need not be a physical quantum mode; it can be a representative removed by an exact relational constraint. The operative sequence is therefore not "construct an indefinite microscopic metric and then remove its ghosts", but

$$\begin{aligned}\text{positive quantum chart} &\longrightarrow \text{exact relational reduction}\\ &\longrightarrow \text{two protected modes} \longrightarrow \text{finite spectral test.}\end{aligned}$$

This sequence is a design rule for finite constrained quantum systems. The body-centred-cubic (BCC) network below is one existence proof, not the principle itself (Fig. 1).

A general protection theorem

Let

$$V_0 \xrightarrow{G} V_1 \xrightarrow{Q} V_2, \qquad QG = 0, \qquad \dim(\ker Q/\operatorname{im} G) = 2 \tag{1}$$

be an exact finite relational complex. After fixing the gauge image, write the remaining coordinates as the direct sum of the physical cohomology $\mathcal{H}$ and the constraint directions $\operatorname{im} Q^{\mathsf{T}}$. Let $K_H \succeq 0$ act on $\mathcal{H}$

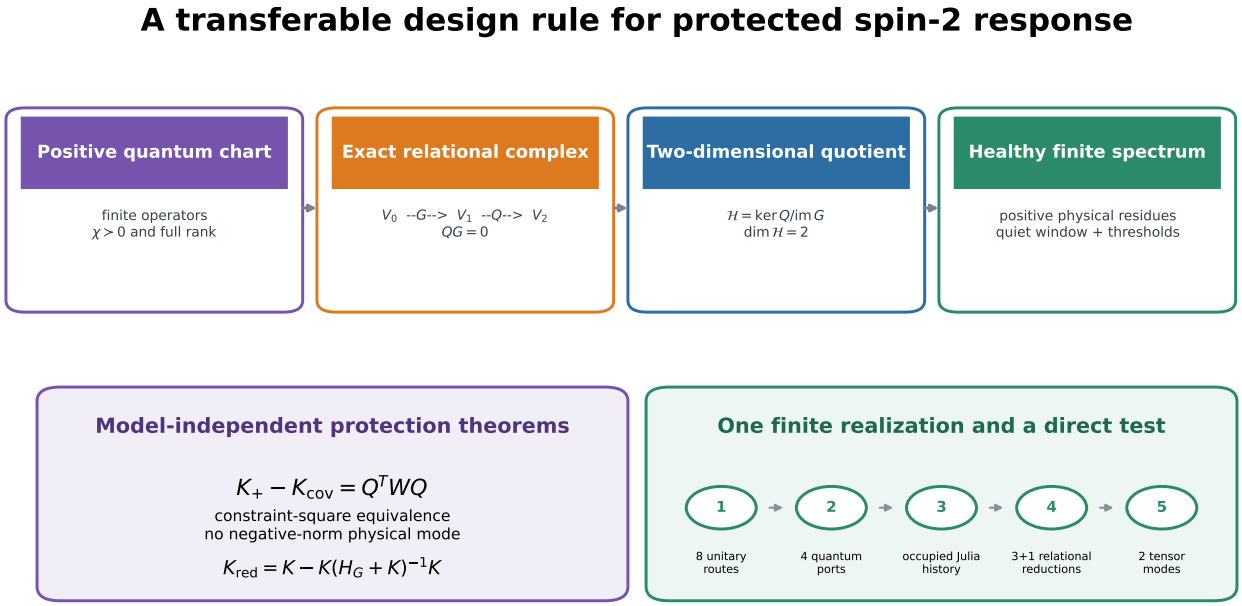


Figure 1: **A transferable design rule.** Positive quantum coordinates are reduced by an exact relational complex before excitations are counted. The general protection identities do not depend on the BCC realization. The explicit network shows that all four design steps can coexist in one finite unitary model and can be tested on a programmable processor.

and let $B, C \succ 0$ act on V_2. The positive response and a covariant representative may be written

$$K_+ = K_H + Q^{\mathsf{T}} B Q, \qquad K_{\mathrm{cov}} = K_H - Q^{\mathsf{T}} C Q. \tag{2}$$

Their difference is

$$K_+ - K_{\mathrm{cov}} = Q^{\mathsf{T}} (B + C) Q. \tag{3}$$

It is a positive quadratic form in the already imposed constraint $Qh = 0$. The two actions therefore have the same constraint surface, reduced equations and physical propagator. If $K_H(p) = p^2 A + O(p^4)$ with $A \succ 0$, both contain exactly two massless positive-residue modes. The negative scalar sign of the covariant representative never becomes a negative-norm state.

This statement is dimension- and graph-independent. We generated 3,000 random exact complexes with $\dim V_1 = 6$–12, constraint ranks 1–9 and positive-chart condition numbers from 1 to 10^{10}. Every realization preserved the two-dimensional quotient and the constraint-square identity to double-precision residuals below 5×10^{-16}. Deliberately breaking exactness produces physical leakage continuously; in the declared ensemble the leakage reaches the 1% gate at an exactness defect of 1.42×10^{-2} (Fig. 2). Thus protection is robust inside an open exact-complex class and fails through a measurable mechanism rather than an arbitrary model change.

A second general result controls the leading quantum correction. Let $H_G \succ 0$ be the Legendre Hessian of a quantum coordinate chart and $K \succeq 0$ its occupied response. Integrating a Gaussian chart fluctuation gives

$$K_{\mathrm{red}} = K - K(H_G + K)^{-1} K, \qquad K_{\mathrm{red}}^{-1} = K^{-1} + H_G^{-1} \tag{4}$$

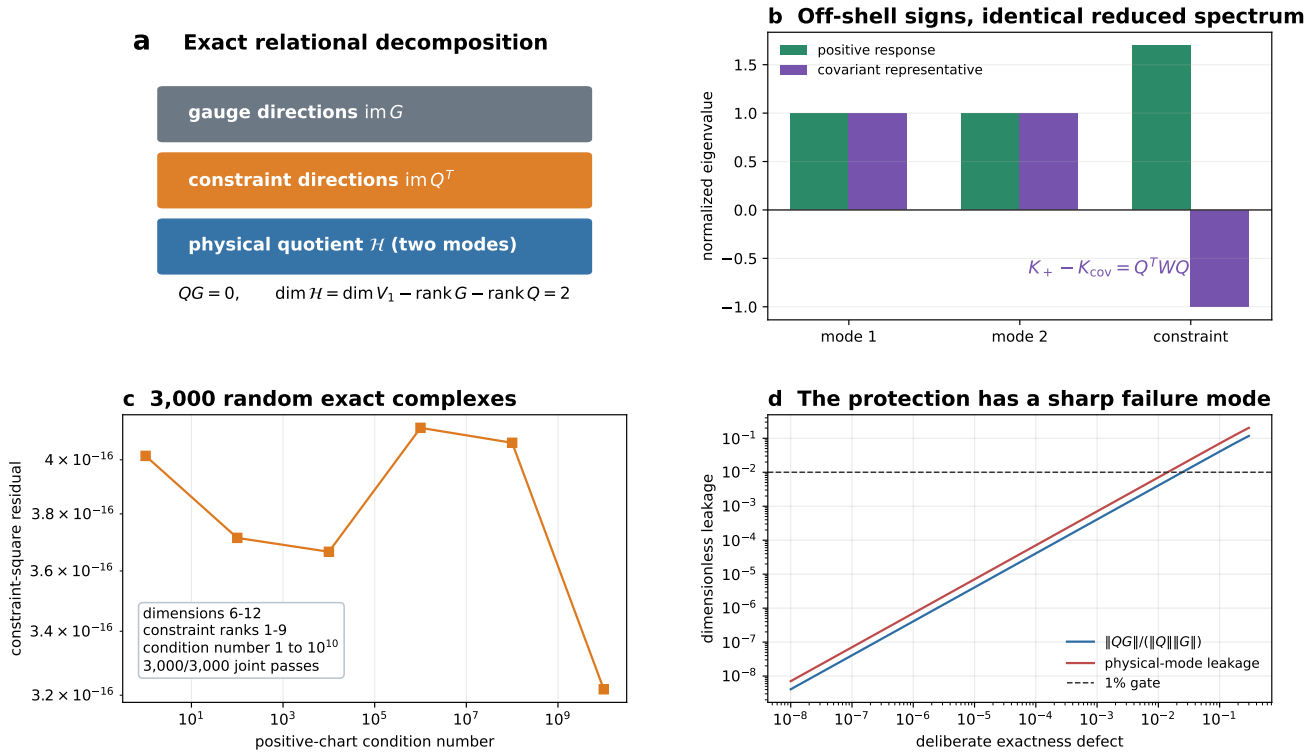


Figure 2: **Constraint protection beyond a specific graph. a**, Exact relational decomposition into gauge, constraint and two physical directions. **b**, Positive and covariant representatives disagree off shell but coincide on the physical quotient. **c**, Random exact complexes preserve the identity across ten decades of chart conditioning. **d**, A controlled defect in $QG = 0$ reopens physical leakage and supplies a quantitative failure boundary.

where the inverse identity holds on the support of K. This matrix parallel sum is positive and has the same kernel as K. For $K(p) = p^2A + O(p^4)$, the correction begins at p^4; rank and masslessness are unchanged. If the physical propagator has a positive Stieltjes spectral measure, adding the analytic positive covariance H_G^{-1} changes zeros but introduces no new poles and leaves inherited residues positive. The hybrid mean field is therefore the leading saddle of a controlled Gaussian expansion, not an untested classical substitution.

One finite unitary realization

The existence proof combines eight oriented BCC routes, a recurrence qubit and four Gauss-invariant quantum ports. Four Casimirs and two shape operators form a six-coordinate Gram chart. In an exact 27-dimensional singlet calibration, its strain covariance is full rank with eigenvalues

$$(0.02431, 0.17014, 0.17014, 0.32176, 0.32176, 0.32176). \tag{5}$$

A relative-cofactor drive removes a common background frame, and a Julia dilation retains the complementary amplitude needed for exact unitarity. Filling the negative-phase branch produces a Gaussian occupied history whose one-channel stiffness is

$$z_{\mathrm{cell}}(m) = \frac{\cos^2 m \, \sin^2 m}{(1 + \cos^2 m)^3} > 0. \tag{6}$$

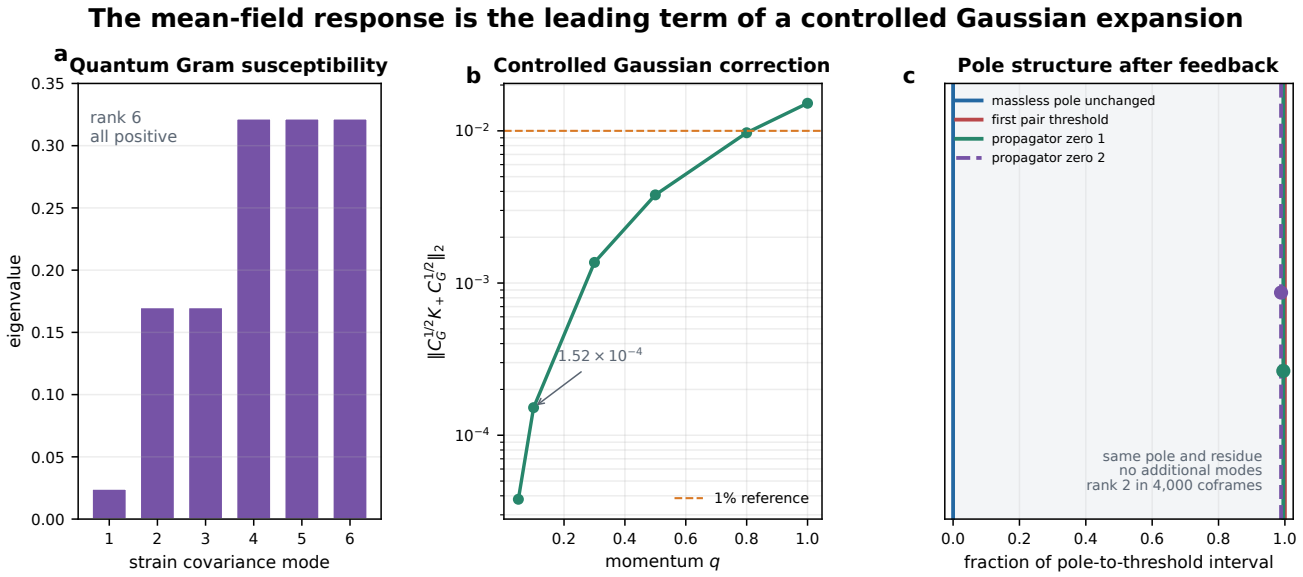


Figure 3: **Controlled quantum-coordinate feedback.** **a**, The exact strain susceptibility is positive and rank six. **b**, The Gaussian expansion parameter stays small in the low-momentum window. **c**, Schur feedback preserves physical poles and residues; the marked near-threshold features are propagator zeros. Random fluctuating coframes preserve the rank-two quotient.

It vanishes when a route is completely open or completely closed, and is positive only when propagation and recurrence coexist.

For non-zero incidence $\boldsymbol{\kappa}$, the network realizes

$$(G_\kappa \boldsymbol{\xi})_{ij} = \kappa_i \xi_j + \kappa_j \xi_i, \qquad Q_\kappa h = (\kappa_i \kappa_j - \kappa^2 \delta_{ij}) h_{ij}. \tag{7}$$

Here $\operatorname{rank} G_\kappa = 3$, $\operatorname{rank} Q_\kappa = 1$ and $Q_\kappa G_\kappa = 0$, leaving plus and cross classes. The positive shell response and the Fierz–Pauli representative differ exactly by the scalar-constraint square in Eq. (3). Repeated finite deformations close on paths rather than on a fictitious site derivative; their matrix generators satisfy the Jacobi identity exactly. These microscopic details establish that the general rule is non-empty.

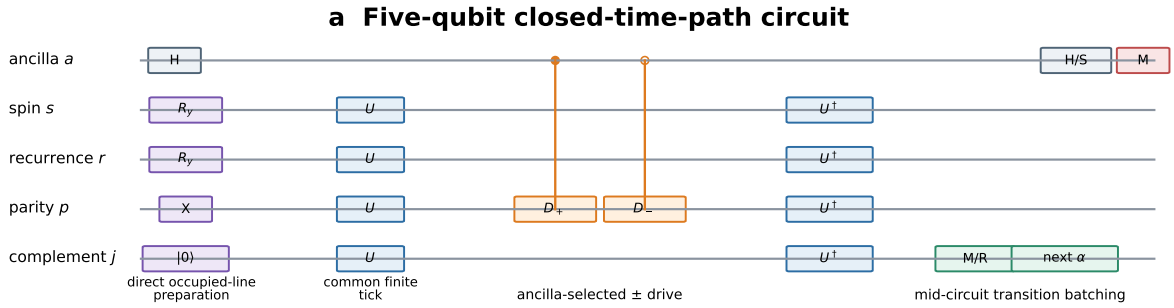
Using the exact Gram covariance in Eq. (4), all six corrected susceptibility eigenvalues remain positive. The two physical propagator poles and residues are unchanged; two near-threshold features are antiresonance zeros, not extra modes. Rebuilding the relational projector on 4,000 fluctuated positive coframes produced no rank failure. The finite-band kernel remains Stieltjes positive, with a quiet interval below the first pair threshold and nonnegative threshold noise (Fig. 3).

A programmable falsification test

The theorem can be tested without assigning the modes a gravitational meaning. A compact circuit uses five logical qubits: response ancilla, spin, recurrence, parity and a reused complementary-route register. Direct occupied-line synthesis is followed by a common finite tick, ancilla-selected plus or cross drives, inverse evolution and ancilla X/Y readout. Ramsey insertions measure two-time correlations and the symmetrized noise; mid-circuit measurement and reset batch the transition channels.

An all-to-all implementation requires 57 native entanglers at estimated entangling depth 39. Mapping the same logical schedule to a declared T-connected superconducting patch gives 123–154 native entanglers and depth 72–96. The dynamic version uses eight mid-circuit measurement/reset operations per transition batch. These operations, conditional branches and parameterized two-qubit rotations are supported by

A near-term falsification test independent of the gravity interpretation



b Architecture-aware resource ledger

Logical register	5 qubits
All-to-all implementation	57 native entanglers; depth 39
T-connected superconducting patch	123-154 native entanglers; depth 72-96
Dynamic batching	8 mid-circuit measure/reset operations
State preparation	direct synthesis recommended; adiabatic circuit is a validation control

Mitigation: assignment correction, Pauli twirling, symmetry verification, dynamical decoupling during MCM, and selected-frequency zero-noise extrapolation.

c Statistical power and non-retunable gates

- pilot scan: 984,000 shots
- 1% helicity comparison: 76,832 shots per helicity (worst case)
- confirmatory total: 3,769,984 shots
- 95% interval for helicity splitting must lie inside ±1%
- subthreshold noise upper bound <1% of first line
- every physical residue has a positive 95% lower bound
- roots interlace thresholds; no scalar/vector response

Figure 4: **Five-qubit test of relational protection.** **a**, Closed-time-path circuit and transition batching. **b**, Architecture-aware resource estimates, including mid-circuit operations and mitigation. **c**, Statistical power and non-retunable acceptance gates. A negative result rejects the finite theorem itself.

contemporary trapped-ion and superconducting architectures, although platform-specific transpilation remains an experimental task[13, 14, 15, 16, 17].

The statistical ledger separates a 984,000-shot pilot scan from confirmatory tests. A worst-case 1% helicity comparison at 95% confidence requires 76,832 shots per helicity; the full declared confirmatory budget is 3,769,984 shots including quiet-window, residue, scalar/vector-control, calibration and selected-frequency zero-noise-extrapolation runs. The model passes only if the 95% interval for plus/cross splitting lies inside ±1%, the subthreshold-noise upper bound is below 1% of the first resolved line, every physical residue has a positive 95% lower bound, roots interlace thresholds and transverse-tensor drives produce no scalar or vector response (Fig. 4). These gates are fixed before hardware execution and cannot be rescued by a continuum interpretation.

The protocol family is not tied to gravity. Replacing the BCC tick and Gram drive by another constrained unitary tests the same design question in engineered gauge systems, topological codes or analogue elastic networks: does a positive microscopic chart descend to a protected low-rank dynamical quotient with a healthy spectral measure?

Finite-kernel fingerprints

The general theorem fixes the protected mode count and signs; ultraviolet coefficients remain realization dependent. For the BCC existence proof, matching any local analytic kernel to the exact response through

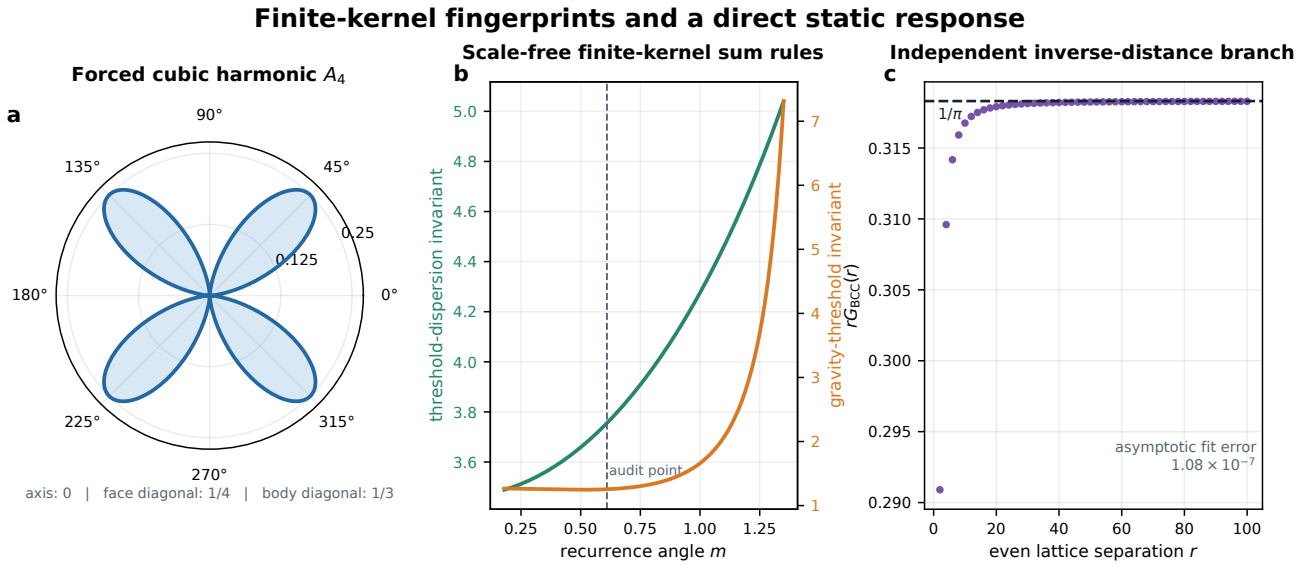


Figure 5: **Fingerprints of the BCC realization. a**, Cubic quartic harmonic forced by the exact finite kernel. **b**, Pair threshold, dispersion length and response normalization obey scale-free correlations. **c**, A direct finite static calculation yields an inverse-distance branch. These ultraviolet details are realization specific; quotient protection is not.

quartic order forces

$$\omega_g^2 = q^2 - \Gamma_{\mathrm{ind}}(m)\,\mathcal{A}_4(\hat{\boldsymbol{q}})q^4 + O(q^6), \quad \mathcal{A}_4 = n_x^2 n_y^2 + n_x^2 n_z^2 + n_y^2 n_z^2. \tag{8}$$

The same kernel fixes scale-free threshold–dispersion combinations, and an independent BCC static Green function approaches $1/(\pi r)$ with relative coefficient error 1.1×10^{-7} (Fig. 5). These are model-level fingerprints that do not require a unique nonlinear Einstein completion. Their coefficients are secondary to the transferable design rule but provide independent checks of the chosen realization.

Scope and design implications

The construction is deliberately hybrid and Gaussian because that level already decides the positive-metric question. Quantum route, port and occupied degrees of freedom are explicit; the coframe is their collective saddle; and its leading quantum feedback is integrated exactly. Non-Gaussian chart–matter entanglement and an anomaly-free operator constraint algebra are the next terms of the programme, not ingredients silently assumed here.

Absolute scales and a realistic matter dictionary are external to this experiment. The BCC harmonic, thresholds and primitive-volume convention belong to the ultraviolet representative, whereas the constraint-square theorem, Schur protection and pole-measure statement hold for the full admissible class. The design principle is consequently stronger than a claim that one lattice reproduces gravity: finite quantum models need not engineer an indefinite microscopic supermetric. They can build positive coordinates, impose relational exactness, reduce before counting excitations and interrogate the complete spectral kernel on hardware.

Methods

Random exact-complex ensemble

For each trial we sampled $\dim V_1 \in [6, 12]$, a gauge rank and a constraint rank compatible with a two-dimensional cohomology. Random orthogonal bases defined mutually orthogonal gauge, physical and constraint subspaces. Positive chart and response matrices were generated with log-uniform condition numbers up to 10^{10}. We checked $QG = 0$, cohomology dimension, Eq. (3), positivity on the physical quotient and Gaussian Schur preservation. A separate family added a controlled component of G in the row space of Q to measure the failure boundary. The random seed and all matrices needed for reproduction are in the machine-readable audit.

Finite realization and Gaussian correction

The BCC route update is the parity-completed Weyl/recurrence unitary. Four Schwinger angular-momentum ports obey Gauss closure; four Casimirs and two pair products form the quantum chart. Relative-cofactor transport and canonical Julia dilation define the source–target history. The occupied projector fills the negative quasienergy branch. The Legendre Hessian is $H_G = B^{\mathsf{T}} \chi_G^{-1} B$, where B maps symmetric coframe strain to centred Gram coordinates. Equation (4) is evaluated analytically and then against the exact finite response. Full definitions and proofs are in Supplementary Information.

Protocol, readout and mitigation

The direct preparation circuit uses three entanglers; an eight-step adiabatic preparation is retained as a validation control, while phase estimation is not required. Retarded response is read from ancilla X/Y contrasts of the forward/backward drive. Symmetrized noise uses ancilla Ramsey two-time correlations; a nine-qubit two-copy covariance circuit is an alternative. The mitigation stack comprises assignment-matrix correction, four Pauli-twirled compilations at fixed total shots, occupied/parity symmetry verification, dynamical decoupling during mid-circuit measurement and three-scale local zero-noise extrapolation at nine selected frequencies. Confidence intervals are bootstrap intervals over circuits and shots. Resource counts are logical scheduling estimates, not claims of completed hardware transpilation.

Data and code

The accompanying archive contains all scripts, JSON outputs, circuit specifications, figure commands and environment files. A permanent public repository identifier should replace the placeholder in the submission system after author deposit.

References

[1] B. S. DeWitt, Quantum theory of gravity. I. The canonical theory, *Phys. Rev.* **160**, 1113–1148 (1967).

[2] M. Fierz and W. Pauli, On relativistic wave equations for particles of arbitrary spin in an electromagnetic field, *Proc. R. Soc. Lond. A* **173**, 211–232 (1939).

[3] A. D. Sakharov, Vacuum quantum fluctuations in curved space and the theory of gravitation, *Sov. Phys. Dokl.* **12**, 1040–1041 (1968).

[4] M. Visser, Sakharov's induced gravity: a modern perspective, *Mod. Phys. Lett. A* **17**, 977–992 (2002).

[5] B. Dittrich and A. Kogios, From spin foams to area metric dynamics to gravitons, *Class. Quantum Grav.* **40**, 095011 (2023).

[6] A. Bisio, G. M. D'Ariano, P. Perinotti and A. Tosini, Weyl, Dirac and Maxwell quantum cellular automata, *Found. Phys.* **45**, 1203–1221 (2015).

[7] P. Raynal, Simple derivation of the Weyl and Dirac quantum cellular automata, *Phys. Rev. A* **95**, 062344 (2017).

[8] A. Barbieri, Quantum tetrahedra and simplicial spin networks, *Nucl. Phys. B* **518**, 714–728 (1998).

[9] J. C. Baez and J. W. Barrett, The quantum tetrahedron in three and four dimensions, *Adv. Theor. Math. Phys.* **3**, 815–850 (1999).

[10] E. Bianchi, P. Donà and S. Speziale, Polyhedra in loop quantum gravity, *Phys. Rev. D* **83**, 044035 (2011).

[11] J. W. York Jr., Conformally invariant orthogonal decomposition of symmetric tensors on Riemannian manifolds and the initial-value problem of general relativity, *J. Math. Phys.* **14**, 456–464 (1973).

[12] G. S. Joyce, Exact results for a body-centred cubic lattice Green function with applications in lattice statistics. I, *J. Math. Phys.* **12**, 1390–1414 (1971).

[13] M. Iqbal *et al.*, Non-Abelian topological order and anyons on a trapped-ion processor, *Nature* **626**, 505–511 (2024).

[14] E. Bäumer *et al.*, Quantum Fourier transform using dynamic circuits, *Phys. Rev. Lett.* **133**, 150602 (2024).

[15] A. Carrera Vazquez *et al.*, Combining quantum processors with real-time classical communication, *Nature* **636**, 75–79 (2024).

[16] D. Hothem *et al.*, Measuring error rates of mid-circuit measurements, *Nat. Commun.* **16**, 5761 (2025).

[17] A. Ransford *et al.*, A 98-qubit trapped-ion quantum computer with all-to-all connectivity, *Nature* **655**, 81–86 (2026).

Supplementary Files

This is a list of supplementary files associated with this preprint. Click to download.

- Relationprotectionspin2quantumsupplementalanon.pdf